Letters

A Novel Finite-Difference Time-Domain Wave Propagator

Funda Akleman and Levent Sevgi

***Abstract*—In this letter, a novel time-domain wave propagator is introduced. A two-dimensional (2-D) finite-difference time-domain (FDTD) algorithm is used to analyze ground wave propagation characteristics. Assuming an azimuthal symmetry, surface, and/or elevated ducts are represented via transverse and/or longitudinal refractivity and boundary perturbations in 2-D space. The 2-D FDTD space extends from $x = 0$ (bottom) to $x \rightarrow \infty$ (top), vertically and from $z \rightarrow -\infty$ (left) to $z \rightarrow \infty$ (right), horizontally. Perfectly matched layer (PML) blocks on the left, right, and top terminate the FDTD computation space to simulate semi-open propagation region. The ground at the bottom is simulated either as a perfectly electrical conductor (PEC) or as a lossy second medium. A desired, initial vertical field profile, which has a pulse character in time, is injected into the FDTD computation space. The PML blocks absorb field components that propagate towards left and top. The ground wave components (i.e., the direct, ground-reflected and surface waves) are traced longitudinally toward the right. The longitudinal propagation region is covered by a finite-sized FDTD computation space as if the space slides from left to right until the pulse propagates to a desired range. Transverse or longitudinal field profiles are obtained by accumulating the time-domain response at each altitude or range and by applying discrete Fourier transformation (DFT) at various frequencies.**

***Index Terms*—FDTD methods, propagators.**

I. Introduction

Ground wave propagation has been and will continue to be one of the important options for communication over long distances near the earth's surface. The model environment is a spherical earth with various ground characteristics, above which exists a radially inhomogeneous atmosphere. Having an excitation and observer anywhere on or above the ground, this model has served as a canonical problem. It is very complex and a full wave numerically computable analytical solution has not appeared yet. Operating frequency, medium parameters (permittivity, permeability, and conductivity) and boundary conditions (geometry) may totally change physical characteristics. For example, while the propagation is limited by the line-of-sight at microwaves, beyond the horizon propagation is possible at high (HF 3–30 MHz) and lower frequencies. The problem, available analytical approximate (ray and mode) solutions and numerical techniques such as split-step parabolic equation (SSPE) have been outlined in [1] together with the hybridization of ray and mode methods. The effects of transverse as well as longitudinal refractivity profiles have also been investigated either analytically [2], [3], or numerically [4]–[6].

Here, a very effective technique is introduced to model various ground wave propagation characteristics. It is a general technique that can be applied to broad range of propagation problems. The technique is based on a two-dimensional (2-D) finite-difference time-domain [7] (FDTD) algorithm, where broad-band pulse propagation is simulated and traced over long distances by a virtual rectangular window that circulates the FDTD space longitudinally back and forth until the range of interest is reached.

Manuscript received August 26, 1999; revised December 2, 1999.

F. Akleman is with the Communication Engineering Department, ITU Electronics, 80626 Maslak/Istanbul, Turkey.

L. Sevgi is with TUBITAK-MRC Information Technologies Research Institute (ITRI), 41470 Gebze/Kocaeli, Turkey.

Publisher Item Identifier S 0018-926X(00)02458-3.

II. A Time-Domain Wave Propagator

The 2-D FDTD wave propagation region and the FDTD computation space are pictured in Fig. 1. The structure is assumed to have azimuthal symmetry. The transverse (x) and longitudinal (z) field components are E_x, H_y and E_z, respectively, which models the classical 2-D TMz ground wave propagation over earth's surface.

Time-domain ground wave propagation over earth's surface is simulated as follows.

- The propagation region (see Fig. 1(a)) is much larger than the FDTD computation space. Therefore, the FDTD computation space covers this region like a moving computation subregion.
- An N_x by N_z (number of transverse and longitudinal cells, respectively) FDTD computation space is terminated by perfectly matched layer (PML) blocks [8], [9] from left $(z \rightarrow -\infty)$, right $(z \rightarrow \infty)$ and $(x \rightarrow \infty)$ top. A perfectly reflecting conductor (PEC) or lossy ground termination is used at the bottom.
- Taking $N_x = 500$ and $N_z = 500$ (total of 250 000 FDTD cells) corresponds to a $50\lambda_{\min} \times 50\lambda_{\min}$ ($\lambda_{\min}$: minimum wavelength) space with a typical $\lambda_{\min}/10$ spatial discretization.
- Various refractivity (e.g., exponential, linear, bilinear or trilinear) profiles over earth's surface is introduced via relative permittivity $\varepsilon_r = n^2(x, z)$.
- Initial altitude profile is injected via the necessary field components. The profile may be a line source or an antenna pattern at a given altitude. Whatever the spatial field distribution, the initial field has a pulse character in time, providing broad-band analysis via a single FDTD run.
- One-way propagation is traced via a 2-D rectangular window as shown in Fig. 1(b). The content of this propagation window is the pulse, which carries information related to the three wave components; direct, ground-reflected, and surface waves.
- This virtual propagation window moves from left to right in FDTD computation space and circulates back to the left when reaches the right-most end, which is the initial profile of the next FDTD computation space. The process and FDTD simulations repeat until the wave longitudinally propagates to a desired range.
- Keeping in mind the number of FDTD cells traced during the circulation of the propagation window, the transverse and/or longitudinal propagation characteristics are obtained.

The direct, ground-reflected and surface waves are traced in time domain, where wave fronts and their interferences (wave maxima and minima) appear as 2-D images. A typical example is given in Fig. 2 for a bilinear refractivity profile. Here, a Gaussian altitude profile is fed as the initial field distribution inside a 500 × 500 FDTD computation space corresponding to 50 m × 50 m physical space (with 0.1 m spatial discretization). The initial field distribution has a pulse character in time (i.e., first derivative of a Gaussian function with 200 MHz bandwidth at 200 MHz center frequency). A 500 × 250 virtual window circulates 20 times as if the longitudinal number of cells in FDTD computation space is 5000. Instant snapshots are taken at different simulation times and are plotted as the field profiles at different ranges. As

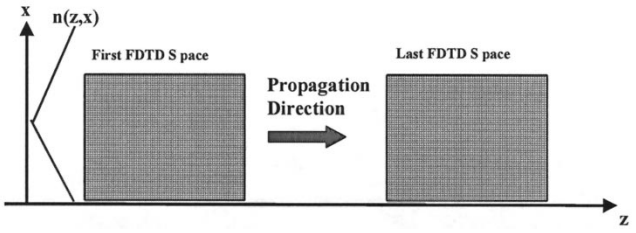

(a)

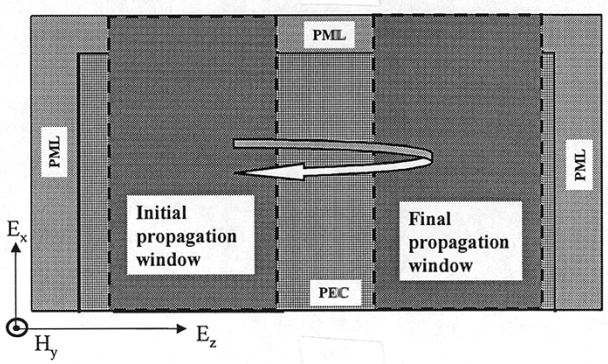

(b)

Fig. 1. (a) The 2-D propagation space. Here, x and z are the transverse and longitudinal coordinates, respectively. A finite-sized FDTD computation space is used as if this region is covered by multi-FDTD computation spaces. (b) Detailed picture of one FDTD computation space. The left, right, and top of this space is terminated by PML blocks to simulate the semi-open propagation region. The bottom is shown to be PEC in this example. A virtual propagation window, which is adjusted to contain the propagation of the initial pulse, slides from left-to-right inside this FDTD computation space. The final window of the current FDTD computation space will be the initial window of the next FDTD space.

shown in the figure, the wave propagates towards the ground and reflects back. The interference of direct and ground reflected waves as well as the surface waves are clearly observed in the figure.

Frequency-domain characteristics can easily be obtained from the FDTD simulations. For example, an altitude field distribution at a given range can be obtained as follows.

- FDTD simulation is performed as explained above and propagation of waves is traced with the sliding rectangular window until the desired range.
- Time-domain propagation data is accumulated at a number of altitude points at the desired range.
- A 2-D array is used to accumulate the transient responses for all altitude points at the desired range.
- The accumulation continues until all the transients disappear at all altitude points.
- After the FDTD simulation, altitude field distribution at any frequency is obtained by off-line discrete Fourier transformation (DFT) analysis.

III. Numerical Application: Wave Propagation Through a Surface Duct

To check the validity of the new time-domain wave propagator a surface duct problem is taken into account. A linearly decreasing refractivity altitude profile (e.g., standard atmosphere) corresponds to a surface duct over planar earth's surface. The earth's curvature may also be included as a perturbation in refractivity [4]. One-way propagation through a strongly trapping surface duct is simulated with the FDTD wave propagator and the results are compared against SSPE solutions.

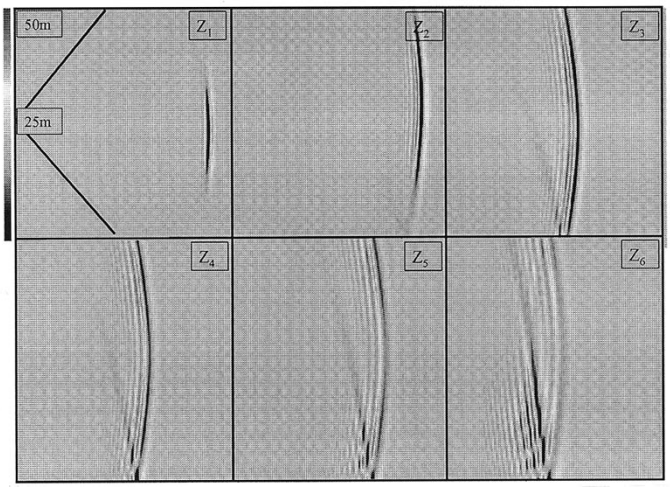

Fig. 2. Time-domain pulse propagation inside the sliding window. $Z_1, Z_1, \cdots, Z_6$ correspond to different propagation ranges. The propagation region is characterised by longitudinally homogeneous, bilinear vertical refractive index with $dn/dx = 10^{-3}$ [n unit/m]. The spatial distribution of the source is Gaussian at an altitude of 25 m. (Z_1: 670th time step, ≈ 50 m range, Z_2: 1570th time step, ≈ 110 m range, Z_3: 2250th time step, ≈ 155 m range, Z_4: 2580th time step, ≈ 180 m range, Z_5: 3070th time step, ≈ 215 m range, Z_6: 4330th time step, ≈ 305 m range).

SSPE is a frequency-domain wave propagator, which is the solution of a parabolic type (PE) wave equation [4]–[6]. It is a one-way propagator that is valid under paraxial approximation (i.e., under weak longitudinal refractivity dependence or under near axial propagation), where backscatter effects are omitted. For a scalar $W(z,x)$ wave function the general solution of SSPE technique is given as

$$W(z,x) = \exp\left[i\frac{k_0}{2}n(z-z_0)\right] \times F^{-1}\left[\exp\left[-i\frac{k_x^2(z-z_0)}{2k_0}\right]F[W(z_0,x)]\right] \quad (1)$$

where $\Delta z = z - z_0, k_0, k_x, \mathrm{FFT}$ and FFT^{-1} correspond to range step size, free-space wavenumber, transverse wavenumber, discrete (fast) Fourier, and inverse discrete (fast) Fourier transforms, respectively. PE is an initial value problem and needs an initial transverse field distribution $W(z_0,x)$. Once supplied, it is longitudinally propagated through a medium defined by its refractive index profile, $n(z,x)$ and the transverse field profile $W(z_0+\Delta z,x)$, at the next range step is obtained. By multi-moving back and forth between x and k_x domains via FFT and inverse FFT the transverse field profile at any range may be obtained [4]–[6].

The results of time- and frequency-domain (FDTD and SSPE) propagators are pictured in Fig. 3. Here, the same transverse (spatial) initial profile is fed into both FDTD and SSPE algorithms and the propagators are run for 500 m. The FDTD propagator is used once and broad band results are obtained. Three of them are shown in the figure. The SSPE propagator needs to be run separately for each frequency. In Fig. 3, the propagation factors ($|E/E_0|$) are plotted. A similar procedure is applied to calculate the propagation factor in both FDTD and SSPE techniques. Both algorithms are run twice. In the first runs, propagation over ground is simulated and E is obtained. In the second runs, they are repeated in free-space (for E_0) and the propagation factors are then obtained. Vertical electric field component is used in FDTD curve, which correspond to Neumann type boundary condition at the surface in SSPE. A good agreement between the results of time and frequency domain wave propagators is clearly seen from the figure.

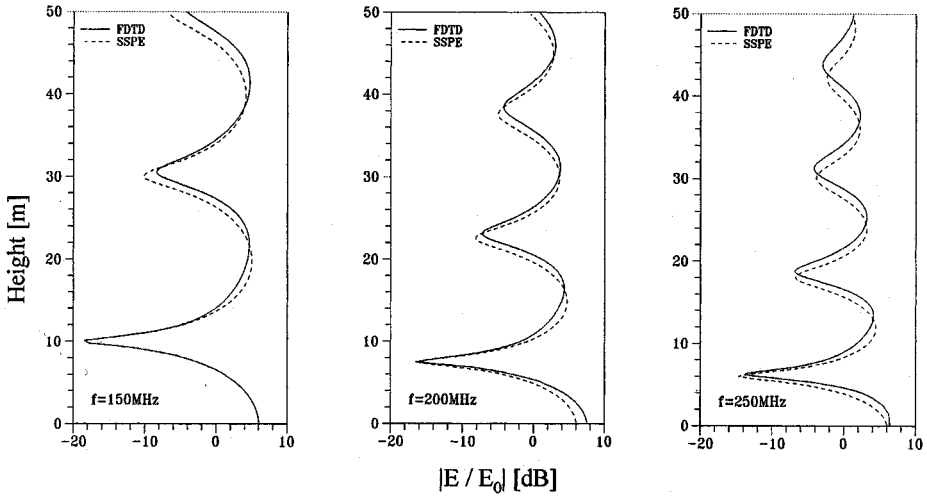

Fig. 3. Altitude field profiles (propagation factors) at 500 m away from the source (corresponding to the ranges of $250\lambda, 330\lambda 415\lambda$ at 150 MHz, 200 MHz and 250 MHz, respectively) obtained via both FDTD and SSPE propagators. The spatial distribution of the source is Gaussian at an altitude of 25 m. The FDTD initial profile is pulse at time (first derivative of Gauss). The SSPE propagator is run separately for each frequency. The propagation region is characterized by longitudinally homogeneous linear vertical refractive index with $dn/dx = 10^{-7}$ [n unit/m].

The FDTD wave propagator is computationally expensive when compared to the SSPE propagator. For example, it takes less than a minute (with a 266 MHZ Pentium PC) in the SSPE simulation to reach the range of 500 m in 800 longitudinal steps when 1024 point FFT is used for the vertical profile. More than an hour of computation time is required to propagate the pulse to the same range with the FDTD algorithm. Although the FDTD simulation time is much more than the other, the SSPE algorithm must be repeated for hundreds of times to give the broad-band propagation information obtained with one FDTD run. It should be noted that no parameter optimization or algorithmic arrangement has yet been done. The memory requirements and computation time will drastically be decreased when optimization is done and when the sliding window size is dynamically controlled.

IV. Conclusion

A novel time-domain wave propagator is introduced in this letter. A 2-D-FDTD algorithm is used for ground wave propagation simulations, where any kind of transverse as well as longitudinal variations can be modeled. Ground losses, terrain effects, and surface roughness can easily be modelled via the new time-domain wave propagator. The technique may also be applied to vertical propagation [10] or any other waveguiding structures [11].

The aim of this letter is to introduce and check the validity of the new time-domain propagator. Although short-range calculations are performed for this purpose in the examples it can easily be extended to long ranges as well as high altitudes, when numerical dispersion requirements are satisfied. Moreover, there is no boundary condition restriction at the surface in the applications. Only long computation times may be required for long range propagation simulations, which may be overcomed by using some intelligent algorithmic and/or parallel processing techniques.

References

[1] L. Sevgi and L. B. Felsen, "A new algorithm for ground wave propagation based on a hybrid ray-mode approach," *Int. J. Numer. Modeling*, vol. 11, no. 2, pp. 87–103, Mar. 1998.

[2] L. B. Felsen and L. Sevgi, "Adiabatic and intrinsic modes for wave propagation in guiding environments with longitudinal and transverse variations: Formulation and canonical test," *IEEE Trans. Antennas Propagat.*, vol. 39, pp. 1130–1136, Aug. 1991.

[3] L. B. Felsen and L. Sevgi, "Adiabatic and intrinsic modes for wave propagation in guiding environments with longitudinal and transverse variations: Continuously refracting media," *IEEE Trans. Antennas Propagat.*, vol. 39, pp. 1137–1143, Aug. 1991.

[4] G. D. Dockery, "Modelling electromagnetic wave propagation in the troposphere using parabolic wave equation," *IEEE Trans. Antennas Propagat.*, vol. 36, pp. 1464–1470, Oct. 1988.

[5] A. E. Barrios, "Parabolic equation modelling in horizontally inhomogeneous environments," *IEEE Trans. Antennas Propagat.*, vol. 40, pp. 791–797, July 1992.

[6] L. Sevgi, "Split step parabolic equation solutions in surface duct-to-elevated duct transition," *Turkish J. Phys.*, vol. 19, no. 3, pp. 541–551, 1995.

[7] K. S. Yee, "Numerical solution of initial boundary value problems involving Maxwell's equations," *IEEE Trans. Antennas Propagat.*, vol. AP-14, pp. 302–307, May 1966.

[8] J. P. Berenger, "A perfectly matched layer for the absorption of electromagnetic waves," *J. Comput. Phys.*, vol. 114, pp. 185–200, 1994.

[9] F. Akleman and L. Sevgi, "A novel implementation of berenger's PML for FDTD applications," *IEEE Microwave Guided Wave Lett.*, vol. 8, pp. 324–327, Oct. 1998.

[10] M. F. Levy, "Horizontal parabolic equation solution of radio wave propagation problems on large domains," *IEEE Trans. Antennas Propagat.*, vol. 43, pp. 137–144, Feb. 1995.

[11] L. Sevgi and E. Topuz, "Split step parabolic equation analysis of coupled dielectric waveguides," *ELEKTRIK, Turkish J. Electron. Commun.*, vol. 3, no. 2–3, pp. 85–92, 1995.

Backscatter Measurements of Thin Nickel-Coated Graphite Fibers

Matthew Hart and C. W. Bruce

***Abstract*—Backscatter cross sections were measured for thin nickel-coated graphite fibers as a function of length. A radiation wavelength of 0.86 centimeters (35 GHz) and fiber lengths varying across the primary resonance spectrum were used. Comparison with recently developed theory shows good agreement, and implications with respect to the effective magnetic permeability are discussed.**

***Index Terms*—Composite material, electromagnetic scattering, graphite fibers, wire scatterers.**

I. Introduction

This experiment is one facet of a more inclusive fibrous aerosol study currently underway at the Army Research Laboratory, White Sands Missile Range, New Mexico. Extinction for nickel-coated fibers and absorption for uncoated graphite fibers have already been reported and show good agreement with theory [1]–[5]. Pertinent contemporary theory includes that of Waterman and Pedersen who have recently published a formulation incorporating a modified current density function for thin, finite length, conductive wires [6] and have extended the theory to include coated wires. In this study we have examined 7.7 μm diameter graphite fibers with a 0.3 μm thick nickel coating with lengths between 3.25 mm and 5.25 mm.

Because the value of the magnetic permeability μ for nickel cannot be assumed to be the dc value for the frequencies of interest, the authors first examined the sensitivity of the backscatter to μ using the theory of [6]. The known dc value for bulk nickel is $50\ \mathrm{N}\cdot\mathrm{A}^{-2}$ and decreases toward unity for frequencies above 10^9 Hz, as has been reported by Allanson *et al.* [7]. Another consideration involves the limited dimensions of the thin conductive coating, which could pose a constraint on the magnetic domains thus effecting μ. Fig. 1 shows the general behavior of the theoretical radar cross section for such fibers at several values of μ at 35 GHz. As will be shown below, experimental data fit best when the value for μ is a number near unity.

II. Experiment

The straight fiber targets were perpendicularly attached at their centers to a thin nylon monofilament that is suspended vertically. The upper suspension point of the line consists of a centering pipet that is able to rotate and is driven with a belt wrap to an electric motor. At the bottom of the line is attached a weight that is sunk into a viscous liquid (glycerin), which dampens vibrations while allowing slow rotation of the line. (It is in this manner that the suspended fibers are rotated in space as data is acquired.) The nylon line passes through a cylindrical container whose interior diameter is 7 in after it has been lined with microwave absorbing material. This container supports the centering pipet and the radiation antenna which is a special horn that serves both as source and receiver (see Figs. 2 and 3). Because of signal to noise considerations a horn was needed that did not have an excessively distant far-field point. The option taken was to flare the waveguide end into a square aperture of approximately one square centimeter. The resultant horn possessed adequate gain with a reasonably close far-field point.

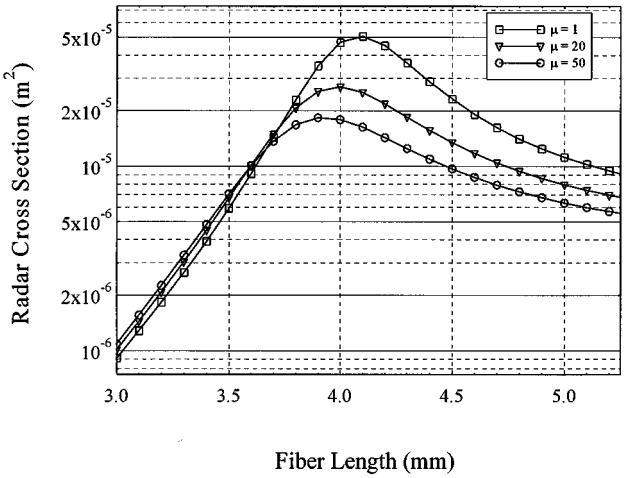

Fig. 1. Theoretical curves for different values of the magnetic permeability μ for an 8.34-μm-diameter nickel fiber.

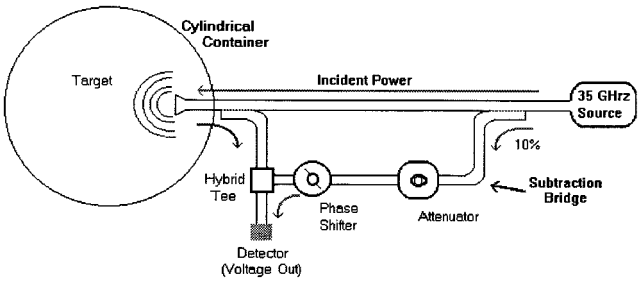

Fig. 2. Basic microwave system used for the backscatter measurements.

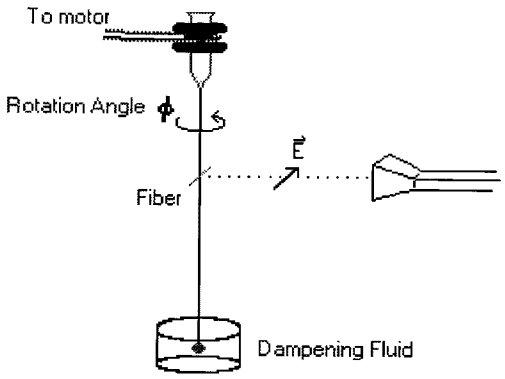

Fig. 3. The fiber mounting arranement.

Reflections back into the waveguide system due to the horn-air interface and the external background can be a source of interference. These static reflections are canceled with the use of a subtraction bridge, which, when properly adjusted, adds a component which is equal in magnitude and opposite in phase, leaving only the received power from the target. (see Fig. 2.) This same apparatus was also recently validated in the process of successfully measuring backscatter from singly falling spheroidal shaped water drops [8].

The incident field is oriented so that the Poynting vector is perpendicular to the monofilament line and is always polarized parallel

Manuscript received August 26, 1996; revised December 11, 1996.

The authors are with the Army Research Laboratory, White Sands Missile Range and New Mexico State University, Physics Department (3D) Las Cruces, NM 88003-0001 USA.

Publisher Item Identifier S 0018-926X(00)04366-0.

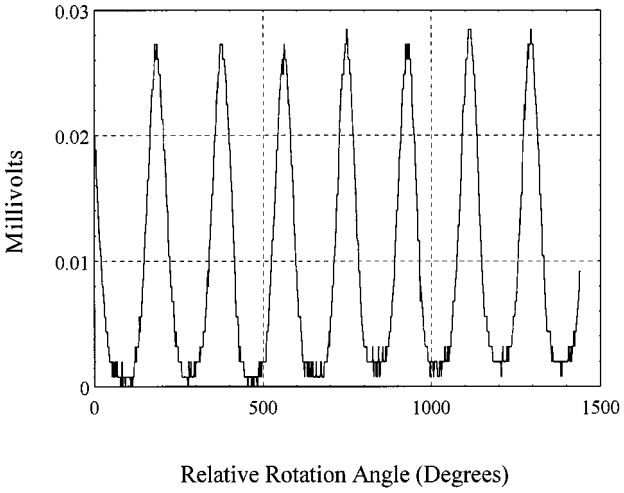

Fig. 4. A typical backscatter signal as the fiber is rotated in front of the antenna.

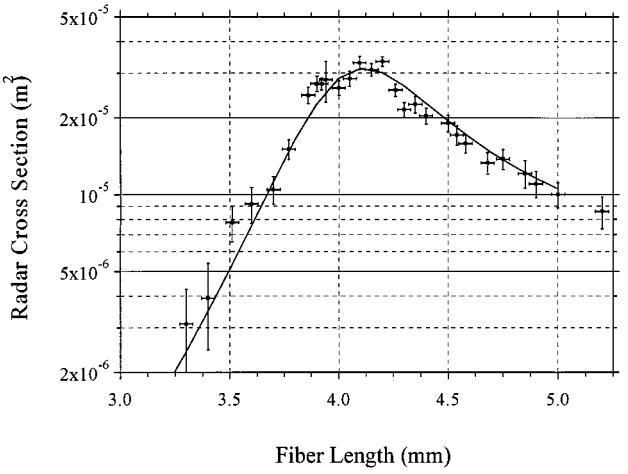

Fig. 5. Measured radar cross sections for 8.0-μm-diameter nickel-coated graphite fibers compared with theory. Here, the magnetic permeability has been set to unity in the theoretical curve.

to the plane of the rotating fiber. Thus, as the nylon filament rotates through the angle ϕ the fiber passes though points of being parallel (strongest field coupling) and perpendicular to the incident electric field (see Fig. 3). Data is acquired as the nylon line rotates. Monostatic backscatter is measured as a function of the rotation angle ϕ. It should also be noted that the symmetry of the nylon line and the system orientation allows for the least possible coupling of incident power to the suspension line. Any possible backscatter from the line is constant during the measurement and can thus be canceled as described above.

A typical data set from a single rotating fiber is illustrated in Fig. 4. The procedure is repeated for different fibers from the same manufacturing lot, but with differing lengths. Normalizing is done by performing a backscatter measurement on a metallic sphere in place of the fiber and then computing an effective incident intensity via Mie theory [9]. The data points correspond to the peak values in Fig. 4 which occur at 180° intervals when the fiber is illuminated at normal incidence. The experimental errors were estimated from the standard deviation stemming from multiple measurements of each fiber.

Out of a total of 54 measured fibers 26 survived the backscatter measurement process and were available for careful analysis of the diameters. In this sampling we found that the average diameter of each was 8.0 μm with a standard deviation of 0.46 μm. Using the given nickel coating thickness of 0.3 μm (which were from the same lot as used by Jelinek [3]) and the measured nickel shell conductivity of $(0.92 \pm 0.05) \times 10^7 1/\Omega \cdot$ m, measured cross section values compare quite well with theory as shown in Fig. 5. In the theoretical comparison curve μ was set to unity which was supplied by Pedersen and represents the most recent application of their theory; that is, scattering from thin, coated, finite-length wires [10]. It should be noted that the nickel conductivity was obtained by means of measurements of dc resistance versus fiber length with the assumption of the above coating thickness and the conductivity of the inner graphite core being approximately three orders of magnitude smaller.

III. Conclusion

The theoretical radar cross sections and the measured values are in close agreement in form. Also, if μ is taken as unity both the amplitude and location of the primary peak agree quite well.

References

[1] C. W. Bruce, A. V. Jelinek, R. M. Halonen, M. J. Stehling, J. C. Pedersen, and P. C. Waterman, "Millimeter wavelength attenuation efficiencies of fibrous aerosols," *J. Appl. Phys.*, vol. 74, p. 3688, Sept. 1993.

[2] C. W. Bruce, D. R. Ashmore, P. C. Pittman, N. E. Pedersen, J. C. Pedersen, and P. C. Waterman, "Attenuation at a wavelength of 0.86 cm due to fibrous aerosols," *Appl. Phys. Lett.*, vol. 56, no. 8, p. 791, Feb. 1990.

[3] A. V. Jelinek and C. W. Bruce, "Extinction spectra of high conductivity fibrous aerosols," *J. Appl. Phys.*, vol. 78, p. 2675, Aug. 1995.

[4] K. P. Gurton and C. W. Bruce, "Parametric study of the absorption cross section for a moderately conducting thin cylinder," *Appl. Opt.*, vol. 34, no. 15, May 1995.

[5] A. V. Jelinek, C. W. Bruce, and K. Gurton, private communication, 1990.

[6] P. C. Waterman and J. C. Pedersen, "Electromagnetic scattering and absorption by finite wires," *J. Appl. Phys.*, vol. 78, p. 656, July 1995.

[7] J. T. Allanson, "The permeability of ferromagnetic materials at frequencies between 10^5 and 10^{10} c/s," *J. Inst. Elec. Eng.*, pt. III, vol. 92, p. 247, 1945.

[8] M. Hart, , Ph.D. dissertation, New Mexico State Univ., Las Cruces, 1996.

[9] C. F. Bohren and D. R. Huffman, *Absorption and Scattering of Light by Small Particles.* New York: Wiley, 1983.

[10] P. C. Waterman and J. C. Pedersen, "Scattering by wires of arbitrary material properties," *IEEE Trans. Antennas and Propagat.*, Feb. 1996.